Robot-Guided Open-Loop Insertion of Skew-Line Needle Arrangements for High Dose Rate Brachytherapy

Animesh Garg, *Student Member, IEEE*, Timmy Siauw, Dmitry Berenson, *Member, IEEE*, J. Adam M. Cunha, I-Chow Hsu, Jean Pouliot, Dan Stoianovici, *Member, IEEE*, and Ken Goldberg, *Fellow, IEEE*

***Abstract*—We present a study in human-centered automation that has potential to reduce patient side effects from high dose rate brachytherapy (HDR-BT). To efficiently deliver radiation to the prostate while minimizing trauma to sensitive structures such as the penile bulb, we modified the Acubot-RND 7-axis robot to guide insertion of diamond-tip needles into desired skew-line geometric arrangements. We extend and integrate two algorithms: Needle Planning with Integer Programming (NPIP) and Inverse Planning with Integer Programming (IPIP) to compute skew-line needle and dose plans. We performed three physical experiments with anatomically correct phantom models to study performance: two with the robot and one control experiment with an expert human physician (coauthor Hsu) without the robot. All were able to achieve needle arrangements that meet the RTOG-0321 clinical dose objectives with zero trauma to the penile bulb. We analyze systematic and random errors in needle placement; total RMS error for the robot system operating without feedback ranged from 2.6 to 4.3 mm, which is comparable to the RMS error of 2.7 mm obtained in an earlier study for PPI-BT treatment using a robot with 3D ultrasound feedback.**

***Note to Practitioners*—Brachytherapy treats cancer by delivering radioactive sources proximal to cancer sites via needles. Current methods use standardized fixed mechanical templates that force needles into parallel arrangements that may prevent needles from reaching prostate volumes blocked by the pubic arch and often require needles to puncture sensitive organs. Skew-line (nonparallel) arrangements of needles can reach targets under the pubic arch and avoid sensitive organs. However, these arrangements cannot be achieved with standard templates, motivating the use of automation. We present a human-centered automation system that integrates state-of-the-art needle and dose planning algorithms with a modified needle insertion robot. Results suggest that the robot can achieve precision and accuracy comparable to that of expert human physician. This approach has applications to brachytherapy treatment for other organs and to other needle procedures such as biopsy and anesthetic injection.**

***Index Terms*—Brachytherapy, health care, needle insertion, prostate cancer, radiation, robot, robot assisted surgery, steerable needles.**

Manuscript received December 15, 2012; revised June 06, 2013; accepted July 25, 2013. Date of publication August 15, 2013; date of current version October 02, 2013. This paper was recommended for publication by Associate Editor Y. Li and Editor M. C. Zhou upon evaluation of the reviewers' comments. This work was presented at the IEEE International Conference on Automation Science and Engineering, August, 2012. This work was supported in part under Grant NIH-1R01EB-006435-01A1, Grant NSF-0905344, Grant NSF-IIS-1227406, and the American Cancer Society under Grant IRG-97-150-13.

A. Garg is with the Department of Industrial Engineering and Operations Research, University of California, Berkeley, CA 94720 USA (e-mail: animesh.garg@berkeley.edu).

T. Siauw, J. A. M. Cunha, I.-C. Hsu, and J. Pouliot are with the Department of Radiation Oncology, University of California, San Francisco, CA 94143 USA (e-mail: siauwk@radonc.ucsf.edu; cunhaa@radonc.ucsf.edu; ihsu@radonc.ucsf.edu; jpouliot@radonc.ucsf.edu).

D. Berenson is with the Department Computer Science, Worcester Polytechnic Institute, MA 01609 USA (e-mail: dberenson@cs.wpi.edu).

D. Stoianovici is with the Department of Urology, Mechanical Engineering, and Neurosurgery, Johns Hopkins University, Baltimore, MD 21224 USA (e-mail: dss@jhu.edu).

K. Goldberg is with the Department of Industrial Engineering and Operations Research, University of California, Berkeley, CA 94720 USA, and also with the Department of Electrical Engineering and Computer Science, School of Information, and the Department of Radiation Oncology, University of California, San Francisco, CA 94143 USA (e-mail: goldberg@berkeley.edu).

Color versions of one or more of the figures in this paper are available online at http://ieeexplore.ieee.org.

Digital Object Identifier 10.1109/TASE.2013.2276940

I. Introduction

EACH year, over 500,000 cancer patients worldwide are treated with brachytherapy [1], where radioactive sources are placed inside the body close to cancerous tumors ("brachys": Greek for "proximal"). Brachytherapy is an effective treatment for cancers in the prostate, cervix, breast, and other anatomical sites [2]. We focus on prostate treatment, where current approaches often result in side-effects such as incontinence and impotence [3]–[5]. Most side-effects result from needle penetration through sensitive structures (urethra, bladder, rectum, penile bulb, cavernous veins, and neuro-vascular bundles) [5]–[9].

There are two forms of brachytherapy: prostate permanent-seed implant (PPI) and high dose rate (HDR). In PPI-BT, needles implant radioactive seeds with a relatively short half-life (weeks) which are left in the patient after the procedure. In high dose rate brachytherapy (HDR-BT), multiple needles are inserted into the patient. After scanning and planning, a highly radioactive source is automatically moved through each needle using a remote afterloader. The dose distribution is controlled by source dwell times at prespecified positions along the needles; the source is removed after treatment. This study focuses on HDR-BT.

In the current approach to prostate HDR-BT, hollow needles are inserted into the prostate through the perineum. The insertion is performed manually by the physician using real-time imaging using a trans-rectal ultrasound probe and a rigid template with parallel holes. As illustrated in Fig. 1 (left), the rigid template requires that all needles be parallel. This restriction often results in puncture of healthy organs such as the penile bulb and related vasculature, and can prevent access to some sections of the prostate due to pubic arch interference. Alternatively, skew-line (non-parallel, non-intersecting) needle

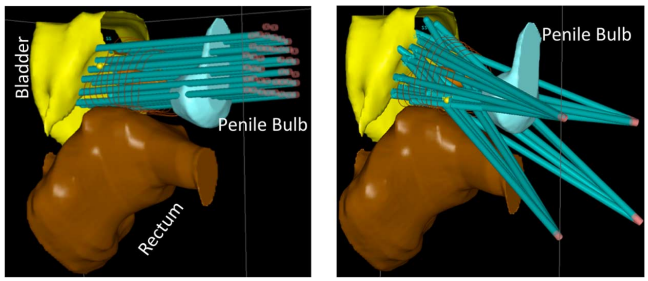

Fig. 1. Left: The current clinical approach to prostate high dose rate brachytherapy (HDR-BT) uses parallel needles guided by a mechanical template. This approach may prevent needles from reaching prostate volumes blocked by the pubic arch and often require needles to puncture sensitive organs (which can produce long-term side-effects). Right: Skew-line needle arrangements facilitated by robot guidance can avoid puncture by reaching under the pubic arch and can minimize trauma to sensitive organs such as the penile bulb which can produce side effects such as incontinence and impotence.

arrangements as shown in Fig. 1 (right), can avoid puncturing delicate structures and be angled to reach under the pubic arch. Recently a "freehand" approach that does not require the template was proposed by physicians to allow skew-line needle arrangements [10]. However, the freehand approach requires a high degree of skill and clinical proficiency. This paper explores the use of a robot to guide skew-line needle arrangements in HDR-BT.

In previous work, we developed the IPIP algorithm to compute HDR-BT dose plans [11] and the NPIP algorithm for computing skew-line needle arrangements [12]. In simulation, we have shown that these algorithms can generate patient-specific skew-line needle arrangements that avoid sensitive organs and meet treatment dose objectives. This study integrates these planning algorithms with the Acubot-RND needle guiding robot [13] illustrated in Fig. 2 (left). Experiments suggest that a human-centered automation system can successfully implant skew-line needle arrangements that avoid puncturing non-prostate structures, meet clinical radiation dose objectives, with mean RMS error between planned and actual dwell points between 2–4 mm.

II. Background and Related Work

Automation can benefit a variety of medical applications: surgical robotics [14], remote diagnosis [15], radiation biodosimetry [16], health analytics [17], and monitored anesthesia control [18]. Okamura *et al.* [19] provides a detailed description of recent advances in medical and healthcare robotics.

The clinical HDR-BT workflow has six main steps: pre-implant patient scanning, needle planning, needle insertion, post-implant patient scanning, dose planning, and dose delivery. Existing research has explored planning systems for computing optimal dose distributions for both PPI- and HDR-BT [11], [20]–[24]. Since the set of possible dose distributions depends on the implanted needle arrangement, planning systems like Prostate Implant Planning Engine for Radiotherapy (PIPER) [20] and Hybrid Inverse Planning and Optimization (HIPO) [24] incorporate the positioning of needles into their dose planning model. However, these approaches were developed for the standard parallel needle template, which has a smaller search space: fewer than 100 candidate parallel needles in contrast to 200–300 candidates for skew-line needles.

In contrast to active needle steering using bevel-tips or cannuli [25]–[31], this study explores how a symmetric (diamond-tip) needle can be steered to a desired configuration within tissue by precisely positioning and orienting its primary axis outside the body.

Prior research in automated needle insertion has explored devices that address the clinical challenges of space constraints and safety requirements for needle insertion robots specially designed for prostate brachytherapy with trans-rectal ultrasound guidance [32]–[35]. Several of these devices can potentially insert skew-line needles, but they focus on PPI-BT and are not fully integrated with needle planners [36]–[40] The Acubot-RND was designed for PPI-BT and is operated by a manual joystick [13], [41], [42]. In this study, we modify the Acubot-RND with an interface to our needle planning software.

A recent study by Long *et al.* [43], used the PROSPER image-guided robotic brachytherapy system [35] to perform multiple needle insertions into a gelatin phantom using intra-operative feedback from a 3-D ultrasound system. As noted in the Discussion section, we obtain similar error values without using ultrasound feedback.

The present study focuses on HDR-BT and integrates automated needle planning system with open-loop robot guided insertion using the Acubot-RND. The needle and dose planning systems are discussed in Section IV and the modifications to the Acubot-RND are discussed in Section V. This is a revised and expanded version of a paper presented at the IEEE International Conference on Automation Science and Engineering (CASE) [44]. This paper is rewritten throughout, with an expanded related work section and detailed analysis of random versus systematic error.

III. Problem Statement

The RTOG-0321 clinical protocol [45] established recommendations for a set of dosimetric indices that are correlated with positive patient outcomes. In these indices, $\mathrm{V}_d^{\mathrm{s}}$, is the volume of structure s that receives at least d percent (e.g., 75%, 100%, 150%) of a specified reference radiation dose (typically 950 cGy).

For the prostate, the value of $\mathrm{V}_d^{\mathrm{Prostate}}$ is specified as a percentage of the total prostate volume, thus $\mathrm{V}_{100}^{\mathrm{Prostate}} >= 90\%$ specifies that at least 90% of the prostate volume should receive at least 100% of the specified reference radiation dose. For other structures such as the bladder, penile bulb, rectum, and urethra, $\mathrm{V}_d^{\mathrm{s}}$ is specified in cubic centimeters, thus $\mathrm{V}_{125}^{\mathrm{Urethra}} <= 0.1$ cc specifies that no more than 1 cc of the urethra should receive more than 125% of the reference dose. The RTOG-0321 recommendations are summarized in the second column of Table I. Note that $\mathrm{V}_{200}^{\mathrm{Body}} = 0$ cc specifies that no non-organ volume of the body should receive 200% of reference radiation dose.

The treatment requires a sequence of steps: A 3D model of patient anatomy is obtained from a CT scan and manually segmented into organs. We then: 1) plan a needle arrangement, if such exists, that lies within the workspace of the robot, avoids non-prostate organs/structures, and meets RTOG-0321 dose requirements; 2) transform this plan into a set of corresponding

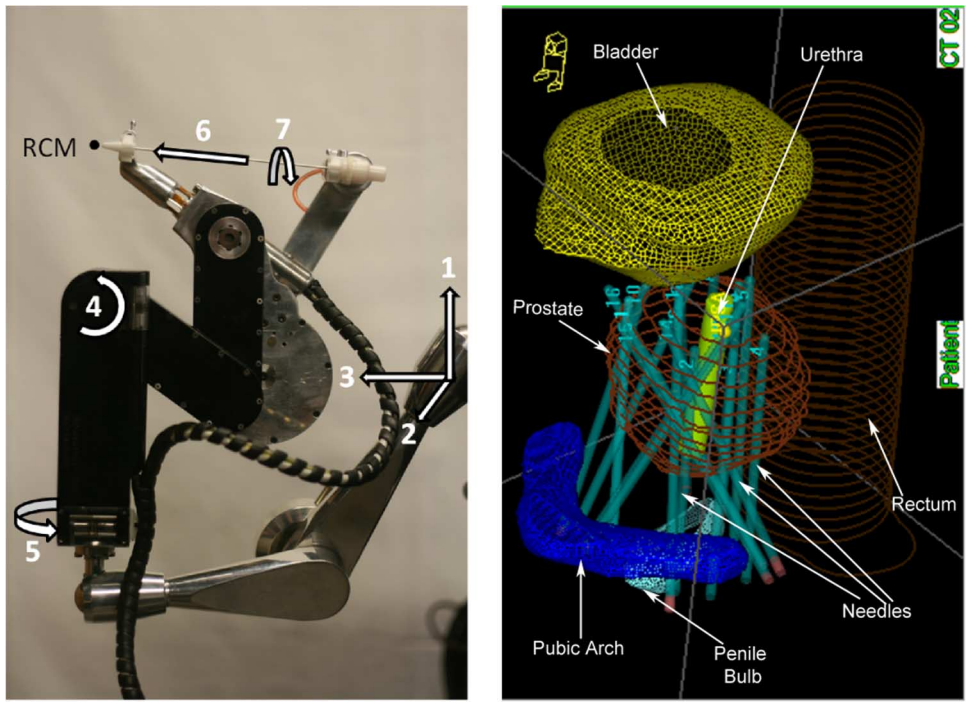

Fig. 2. The left figure shows the 7-DoF Acubot-RND robot used for this study. It has a 3-DoF Cartesian stage (1, 2, and 3), a two DoF rotating center of motion (4 and 5), needle insertion (6) and needle rotation (7). The right figure shows a skew-line needle arrangement implanted by the robot system into a phantom as viewed after CT-Scan.

TABLE I
LISTS THE CLINICAL DOSE INDEX AND TRAUMA METRICS, THE RTOG-0321 REQUIREMENTS, AND THE VALUES FROM EACH EXPERIMENT, PH1 AND PH2 USING THE ROBOT, AND PH3 BY AN EXPERT HUMAN PHYSICIAN. COLUMNS P1 AND A1 ARE THE DOSE VALUES ACHIEVED BY IPIP FOR THE PLANNED AND ACTUAL NEEDLE ARRANGEMENTS, RESPECTIVELY, FOR PH1. THE SAME FOR P2, A2, AND PH2. A3 FOR THE THIRD PHANTOM PH3 IS BASED ON THE NEEDLES AS ACTUALLY IMPLANTED BY THE EXPERT HUMAN PHYSICIAN (WHO DID NOT PLAN A NEEDLE ARRANGEMENT)

		Phantom 1		Phantom 2		Phantom 3
Metric	RTOG Req.	P1	A1	P2	A2	A3
$V_{100}^{Prostate}$	$\geq 90\%$	99.0	97.0	96.0	96.0	98.0
$V_{150}^{Prostate}$	$\leq 45\%$	39.0	40.0	40.0	37.0	37.0
$V_{75}^{Bladder}$	≤ 1 cc	0.00	0.00	0.30	0.80	0.30
$V_{100}^{Bladder}$	= 0 cc	0.00	0.00	0.00	0.00	0.00
V_{75}^{Bulb}	≤ 1 cc	0.00	0.00	0.00	0.00	0.00
V_{100}^{Bulb}	= 0 cc	0.00	0.00	0.00	0.00	0.00
V_{75}^{Rectum}	≤ 1 cc	0.06	0.00	0.00	0.00	0.00
V_{100}^{Rectum}	= 0 cc	0.00	0.00	0.00	0.00	0.00
$V_{125}^{Urethra}$	≤ 0.1 cc	0.06	0.05	0.04	0.06	0.07
$V_{150}^{Urethra}$	= 0 cc	0.00	0.00	0.00	0.00	0.00
V_{200}^{Body}	= 0 cc	0.00	0.00	0.00	0.00	0.00
T^{Bulb}	min	0.00	0.00	0.00	0.00	0.00

robot set-points so that each needle starting position and orientation guides a human novice who inserts needles to the indicated depth; and 3) perform a second CT scan, compute a dose plan for the actual needle arrangement and report RTOG-0321 dose indices.

To quantify the damage to sensitive organs and structures, we propose a trauma metric equal to the total intersection volume: The trauma metric for structure s is

$$T^s = \sum_k A_k L_k^s,$$

where A_k is the cross sectional area of needle k and L_k^s is the length of needle k puncturing structure s. The needles have a circular cross sections, hence, $A_k = \pi d^2/4$ in mm^2, where d is needle diameter.

IV. PLANNING SKEW-LINE NEEDLE ARRANGEMENTS AND DOSE DISTRIBUTIONS

To plan skew-line needle arrangements and dose plans, we modified the needle planning with integer programming (NPIP) needle planning algorithm [12] to use a more comprehensive sample set of candidate needles and we incorporated it with the IPIP dose planning algorithm [11]. These references include details on these planners with experiments and sensitivity analysis.

NPIP accepts as input patient anatomy, the prostate target, obstacles such as the pubic arch and penile bulb, and the defined needle entry zone to search for an arrangement of skew-line needles that: 1) includes approximately 16 needles (the standard at the UCSF clinic); 2) avoids the pubic arch bone and other sensitive organs; 3) offers dwell points that can deliver a dose plan that meets RTOG-0321 dose objectives; and 4) minimizes for the trauma metric.

The planner uses integer programming: it is not complete (guaranteed to find such an arrangement if one exists) nor does it always produce an optimal solution. NPIP was modified to use non-uniform sampling to generate the candidate needle set and an additional constraint: all needles in the solution must have mutual clearance of γ. The parameter γ specifies the distance between the medial axes of a pair of needles. For a non intersecting needle pair, $\gamma \geq d$, where d is the needle diameter. We chose a conservative value of $\gamma = 2d$ to allow for deviations during insertion.

The prostate volume is discretized into a rectangular grid of sample points, with spacing of 4 mm in the x- and y-directions and 3 mm in the z-direction (the interplane CT sample distance). This produced approximately 1000 points for each case. NPIP takes as input this set of sample points and a user-specified parameter, δ. NPIP generates a candidate needle set (line segments) and searches for a subset of these candidate needles where every point within the prostate is within δ of at least one needle. A high value of δ allows needles to cover more volume, producing needle arrangements with fewer needles. To normalize across prostate volume, we set $\delta = 33\%$ of the radius of a sphere with equivalent volume to the prostate and iteratively increased or decreased it to obtain a solution with 16 needles. NPIP uses heuristics to solve an integer program so there are no time or performance guarantees, but for the cases we considered, NPIP computes solutions within 120 s (see Section VI).

The needle arrangements computed by NPIP are given as input to the Inverse Planning by Integer Program (IPIP) dose planning algorithm [11]. Given the set of needles, IPIP computes a set of dwell times (spaced 5 mm apart within each needle) for the radioactive source that maximize $V_{100}^{\text{Prostate}}$ subject to the RTOG-0321 dose requirements. For the three phantom cases we studied, IPIP found solutions within 10 s with values as reported in Table I.

V. The Acubot-RND Robot

The Acubot-RND robot system was designed and constructed at the Johns Hopkins University to guide needle insertion for permanent-seed (PPI-BT) treatment [13]. Hardware specifications for the Acubot-RND, including spatial resolutions and maximum ranges for each degree of freedom are reported in [34].

A. Robot Guided Needle Insertion

As shown in Fig. 2 (left), the Acubot-RND is a 7-DoF robot with three stages: The first is the 3-DoF Cartesian Positioning Stage (CPS), the second is the 2-DoF Rotating Center of Motion (RCM) that sets needle angle keeping the needle tip position fixed, and the third is the 2-DoF Rotating Needle Driver Module (RND) that can rotate and insert needles automatically.

The phantom is draped during the experiments. For this study we position the first stage manually during calibration and we send computed commands to the second stage to orient the needle prior to insertion. We then send a command to the third stage to insert the needle to a prespecified end point without feedback. At this point a human novice (coauthor Garg, an IEOR graduate student with no clinical experience) manually retracts each needle leaving behind a stylet in tissue.

B. Digital Interface

The needle entry plane with CT marker defines the coordinate frame. We modified the Acubot-RND, augmenting the manual joystick operation with a digital interface that allows commanding specific offsets in tip position from the center of the entry zone, and specific pairs of angular offsets from the normal to the plane of needle entry zone.

A needle plan defines a set of i needles, each specified with two points: $\underline{\mathrm{p}}_0^i$ in the entry plane, and $\underline{\mathrm{p}}_1^i$ at the desired distal tip of the inserted needle, where x and y components of $\underline{\mathrm{p}}^i$ span the entry plane in horizontal and vertical directions; and the z component points into the phantom volume. The insertion depth for needle i is d_i, the Euclidean distance between the points. The angles for angle needle i, defined as rotations in the associated planes are

$$\theta_{xz} = atan2\,(x_1 - x_0, z_1 - z_0)$$
$$\theta_{yz} = atan2\,(y_1 - y_0, z_1 - z_0).$$

These angles are specified as joint angles for the RCM.

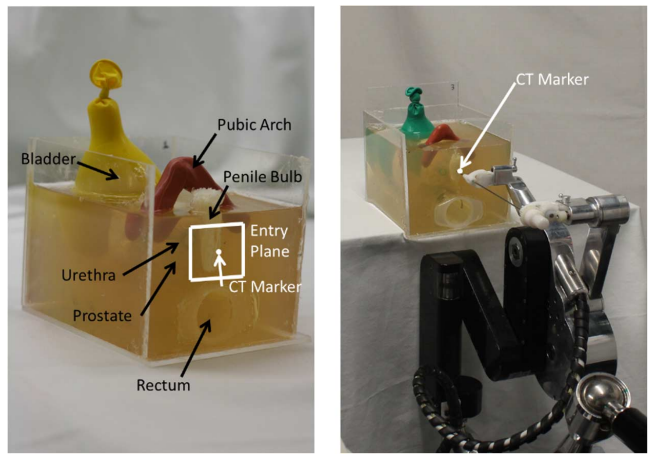

Fig. 3. Prostate phantom (5 in $\times$ 5 in $\times$ 8 in) (left) and insertion setup (right). The anatomy modeled in the phantom includes: prostate; urethra; bladder; penile bulb; pubic arch; and rectum. A CT marker is centered on the square entry zone for calibration. As shown in the right image, the Acubot-RND is registered to the CT-marker.

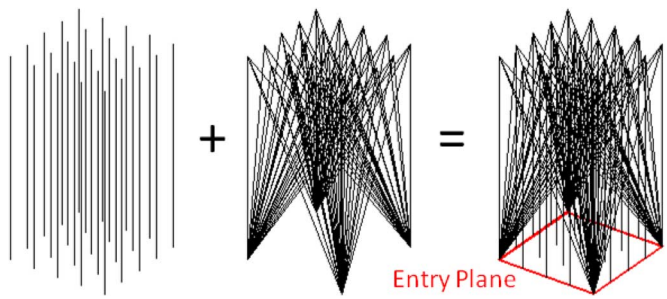

Fig. 4. The candidate needle set is the set of needles that are available during needle planning. As shown in the figure, the candidate needle set for this study consisted of: parallel lines, and skew-lines. The entry plane, which represents the bounded region on the perineum within which needles can enter the phantom is also depicted.

VI. Physical Experiments

To evaluate the performance of the NPIP and IPIP algorithms and robot hardware, we constructed three nearly identical physical phantoms in the clinic at UCSF: Ph1, Ph2, and Ph3. Each includes anatomically correct organ structures of similar density as human tissue and suspended in a translucent gelatin medium. Harder bone structures like that of the pubic arch is constructed from modeling clay. The organ structures include urethra, prostate, bladder, penile bulb, pubic arch, and rectum, as shown in Fig. 3. The square entry zone has dimension 45 mm, consistent with clinical practice, as shown in Fig. 3, relative to an example candidate needle set in Fig. 4.

We performed end-to-end needle insertion procedures with 16 needles on each phantom using the robot for the first two (Ph1 and Ph2) and an expert human physician for the third phantom (Ph3).

Each experiment includes these steps (with step 2 omitted for the expert human physician who used his clinical intuition to determine a needle plan).

1) Perform first CT-Scan and 3D segmentation of organs.
2) Plan desired Needle configuration using NPIP and calculate dose plan IPIP.
3) Implant Needles with robot or with expert human.
4) Perform second CT-scan of phantom with needles.
5) Perform dose planning using IPIP.

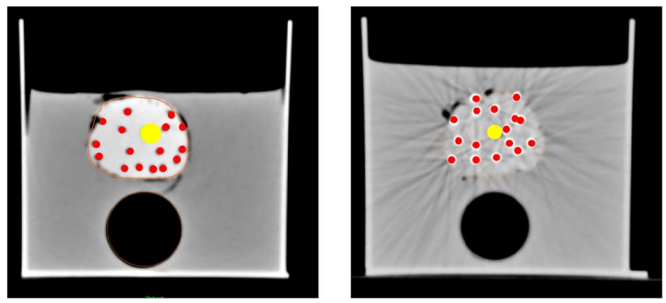

Fig. 5. Cross-sectional view of an actual needle arrangement inserted by an expert human physician without the robot (left) and one inserted by a novice human guided by the robot (right). Both are considered successful as they meet the RTOG dose objectives without penetrating the penile bulb.

A. Robot Experiments

A side view of an implanted phantom Ph1 is shown with needle configuration A1 in Fig. 6. Robot-assisted implant of needles was performed on two phantoms, Ph1 and Ph2. The needle entry zone is a square on the surface of the phantom centered on the CT marker. As in typical clinical cases, the entry zone is 45 mm $\times$ 45 mm, as shown in Figs. 3 and 4. We place a radio-opaque CT-marker at the center of each entry zone to register the coordinate system of the planning algorithm with the robot.

1) Pre-Implant Scanning and Planning: CT scans of tissue phantoms, before and after all 16 needles are inserted, were taken in 3 mm thick slices. The contoured prostate volumes for the three phantoms were 39 cc, 32 cc, and 37 cc. The total phantom volume was 750 cc.

The organs of the phantom and the CT marker were contoured in 3D using the Nucletron Oncentra Dynamic Planning Environment. Using Oncentra, we added a 2 mm margin to the outer contour of the penile bulb. These 3D organ models were exported to NPIP and IPIP. A reference dose of 950 cGy is commonly prescribed for prostate HDR-BT; we used this level as reference in all cases.

For Ph1 and Ph2, there were 287 and 229 candidate needles, respectively. NPIP used a δ value of 6.5 mm for Ph1 and 6.0 mm for Ph2 to produce solutions with 16 needles. γ value was chosen tobe twice the needle diameter, 4 mm. For Ph1 and Ph2, we define two needle arrangements the planned needle arrangements, P1 and P2, and the actual needle arrangements, A1 and A2.

All computation was performed using Matlab R2011a on a Lenovo ThinkPad with an Intel i5-2410M processor and 4 GB of RAM. The integer program optimization was done using the Matlab interface for the Mosek Optimization Toolbox v.6. The complete run for planning using NPIP less than 70 s for both Ph1 and Ph1; and IPIP runs took 10 s for both Ph1 and Ph2.

2) Robot Experiments on Ph1 and Ph2: After the initial CT scan, the robot and phantom are clamped to a worktable, leveled, and manually calibrated as follows: 1) the robot is manually moved to an initial state with first needle tip at the registration mark and aligned normal to the entry plane by moving to specified x and y offsets and confirming that it just touches the surface at each point. Fig. 3 shows the Acubot-RND and phantom in such an initial state. We used a standard 18-gauge diamond-tip brachytherapy needle (COOK Biotech) of length 15 cm and 2 mm diameter hollow sheath that housed a rigid stylet. To implant needle arrangements in Ph1 and Ph2, the Acubot-RND was brought into each specified position and orientation where a needle was inserted by the robot until the prespecified depth in phantom tissue. The insertion depth was marked on a stylet and it was manually pushed through the hollow needle in the phantom by the novice operator, and needle is retracted to leave the stylet in the phantom. The stylets were used as a proxy for needles in phantom to minimize interference to robot during subsequent needle insertions.

3) Expert Human Physician Experiment on Ph3: Co-author Dr. I-Chow Hsu is a certified radiation oncologist at UCSF with a specialization in brachytherapy and over 18 years of clinical experience. He performed insertion on Ph3 for comparison. We performed a CT scan of Ph3 as above. Dr. Hsu used his expert intuition to determine a needle plan. He inserted 16 standard HDR-BT needles into phantom Ph3 under trans-rectal ultrasound (TRUS) guidance using the UCSF-developed "free-hand" technique [10]. A HAWK 2102 EXL TRUS system from B-K Medical was used for ultrasound imaging.

4) Post-Implant CT Scan: After executing all implants, another CT scan is performed on the phantom. The needles are segmented and organs are contoured to determine the needle configuration actually implanted, A_i.

VII. Results

The RTOG-0321 clinical requirements and results from all three experiments, planned and actual for the robot, and actual for the human, are summarized in Table I. For all three cases, clinical requirements were met and performance with the robot was comparable to that of an expert human physician.

The expert human physician experiment was completed in under 15 min. Each robot experiment required approximately 45 min due to calibration and slow needle insertion speeds by the novice. We also note that the expert human physician had the benefit of ultrasound feedback while the needle insertions for the robot experiments were performed without ultrasound or visual feedback.

Fig. 5 shows cross section of the needle arrangements implanted by the expert (left) and by a novice with the robot guide (right).

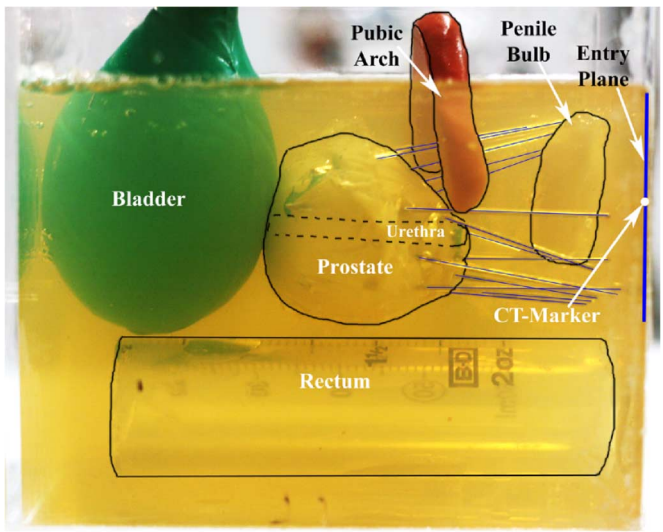

Fig. 6. Anatomically correct phantom Ph1 with robot-implanted needle configuration A1. The organ boundaries and actual needles positions are highlighted. All sensitive structures were spared needle puncture.

TABLE II
ERROR ANALYSIS: TOTAL ERRORS ARE RMS ERRORS (IN MM) MEASURED IN PHANTOMS POST-IMPLANT. RANDOM ERRORS ARE RMS ERRORS (IN MM) AFTER COMPENSATION FOR SYSTEMATIC ERROR. THE x-, y- AND z-ROWS LIST RMS ERRORS IN EACH DIRECTION. d IS THE OVERALL RMS ERROR. SYSTEMATIC ERRORS ARE OBTAINED BY LEAST SQUARE POINT SET MATCHING. (ϵ_i IN mm AND ANGLES IN *degrees*)

	Phantom 1			Phantom 1		
Total RMS	Min	Max	Mean	Min	Max	Mean
x	0.5	2.5	1.4	0.8	2.7	1.9
y	0.2	2.5	1.6	0.7	3.2	2.3
z	0.1	3.0	1.5	0.9	5.3	3.1
d	1.3	4.1	2.6	2.0	6.3	4.3
Random						
x	0.0	0.8	0.5	0.1	2.3	1.2
y	0.1	1.1	0.5	0.1	1.8	1.1
z	0.1	2.3	1.2	0.0	5.1	1.8
d	0.2	2.5	1.4	0.8	5.2	2.4
Systematic						
ϵ_x	1.2			0.9		
ϵ_y	1.4			2.2		
ϵ_z	0.8			2.4		
α	1.8			1.3		
β	−0.9			0.8		
γ	1.6			3.5		

Table I lists the clinical dose index and trauma metrics, the difference between the values obtained from planned versus actual needle arrangements are relatively minor. An exception is the difference in V_{75}^{Bladder} values for P2 and A2 which were 0.3 and 0.8 cc, respectively. They are both below the clinically acceptable limit for this criterion: 1 cc. This discrepancy is due to some needles not being inserted far enough into the prostate. This is mainly due to placement error in manual step of the needle insertion. Since no dwell positions are available at the apex of the prostate, IPIP increases the dwell times at the distal ends of the needles to achieve coverage, but this produces a higher-than-desired dose to the bladder.

Although actual needles could puncture the penile bulb due to placement error, the puncture volume in all planned and actual cases, for the robot and the human, was zero (0 cc). Also, no needles intersected the pubic arch.

Robot Placement Error: We next consider the total, systematic, and random errors between planned and actual needle arrangements in the two robot experiments (there is no planned needle arrangement for the third experiment). We sample needle position at 1 millimeter intervals producing 60 sample points per needle. We use same sampling procedure for planned and actual needle configurations. Hence, using all needles in the arrangement, we generate two sets of corresponding points: a set of planned points P and set of actual points A.

The total error in mm between any pair of planned and actual points is the distance between them. Table II summarizes mean, min, and max RMS error (RMSE) along each dimension and d, the Euclidean distance. The total placement error is the RMS distance over all planned and implanted needle points. For Ph1 and Ph2, the total RMS errors were 2.6 and 4.3 mm, respectively.

We decompose total error into systematic and random components by computing the least-squares rigid transformation between the pairs of point sets [46]. Specifically, we compute the rotation matrix, R, and the translation vector, T, which minimizes the least-squares error over the whole point set

$$\sum \|P - (RA + T)\|_2$$

where P is the vector of planned points and A is the vector of actual points. The associated translations and rotation values define the systematic error. The α, β, and γ values are the rotations in the Euler angles reported in degrees. The Euler angles are computed as

$$\alpha = \sin^{-1}(r_{1,3}),\ \beta = \cos^{-1}\left(\frac{r_{1,1}}{\cos(\alpha)}\right),\ \gamma = \cos^{-1}\left(\frac{r_{3,3}}{\cos(\alpha)}\right)$$

where $r_{i,j}$ is the element of R in the ith row and the jth column. The errors for Phantom 1 and Phantom 2 are shown in Table II.

The random error is the residual error after the actual points are compensated by the least square transformation. Note that systematic and random components do not sum to the total error due to rotations.

Total random error for Ph1 and Ph2 are 1.4 and 2.4 mm, respectively. Table II summarizes the results.

The superposition of the planned (blue) and implanted (red) needles is shown in Fig. 7, as well as the planned and adjusted needle arrangements (green).

VIII. DISCUSSION AND FUTURE WORK

This paper describes the system architecture, algorithms, hardware, and experiments with a human-centered automation system for inserting skew-line needle arrangements for HDR-BT. We report results with an open-loop robot guide system that uses CT scans before insertion and does not use sensor feedback during insertion, and results from an experiment performed by an expert human physician using ultrasound guidance. These results, in a controlled experimental setup with phantom tissues, suggest that skew-line needle arrangements

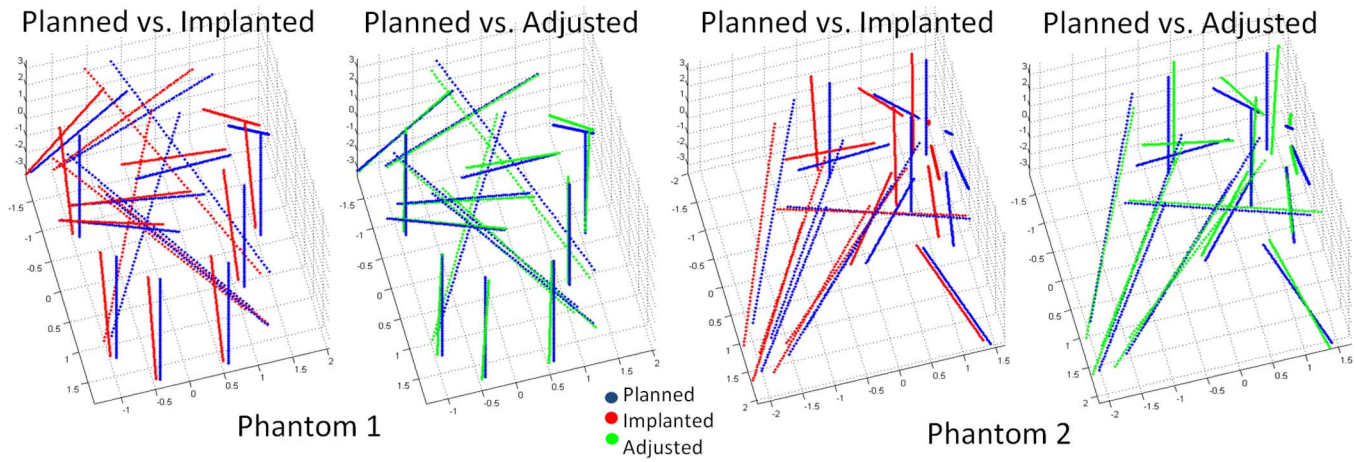

Fig. 7. Superposition of planned (blue) and implanted (red) needle arrangement for Phantom 1 and Phantom 2. Although no sensitive structure was punctured in the implanted needle arrangement and all dose objectives were met, there was nonzero placement error. The placement error was separated into systematic and random error. Upon compensation for the systematic error, the adjusted needle arrangement (green) fits better to the planned configuration.

can be planned and executed with a robot guide to achieve the RTOG-0321 clinical treatment objectives, while avoiding puncture of sensitive structures such as the penile bulb.

Long *et al.* [43] used the PROSPER robot system (developed for PPI-BT), to insert glass bead markers into a gelatin prostate phantom. After an initial insertion, the needle tip and target bead were measured using 3D ultrasound and needle tip was adjusted along the insertion axis until error was minimized. Using such intra-operative feedback, the PROSPER system achieved position errors of 2.7 mm. This error, between needle tips and target points, is relevant for PPI-BT. For HDR-BT, we report RMS error along the entire needle which contains dwell positions. We were able to achieve RMS errors of 2.6 and 4.3 mm, which are comparable to the error achieved in the closed-loop PROSPER system. In future work, we will perform additional experiments with more complex anatomy, for example, enlarged prostates where it may be difficult to avoid pubic arch interference and to treat cancers in other organs. We will study how NPIP and IPIP may be enhanced with higher resolution sampling, where cloud computing may make it feasible to compute plans that are more robust to uncertainty in anatomy and needle motion.

We will also explore how calibration can be enhanced with additional CT markers to reduce systematic error and perform experiments to explore how needle insertion order and needle rotation (rifling) may affect needle insertion accuracy. We will also explore how feedback control can be used during insertion.

Some studies like [47] and [48] have explored use of MRI for real-time scanning. Tovar-Arriaga *et al.* [49] and Ji [50] proposed workflows for needle insertion using CT and MRI feedback, respectively. References [51] and [52] have studied accuracy of needle placements in real-time MRI tracking. Real-time feedback from either CT or MRI has to deal with tradeoff between spatial resolution and temporal resolution. CT can be used for feedback, but it results in radiation exposure to patient. MRI (magnetic resonance imaging) is relatively slow, requires that all needles and guiding equipment be non-ferrous, and has issues with image warping in larger imaging volumes. As Ultrasound is safe and provides real-time imaging, we will explore how it can be incorporated for active needle guidance.

Acknowledgment

The authors would like to thank G. Fitchinger for his work on building the Acubot-RND and the staff at the University of California San Francisco (UCSF) Helen Diller Family Comprehensive Cancer Center and N. Zhang, Y. Zuo, and H. Siao for their assistance in experiments.

References

[1] J. Valentin *et al.*, "Prevention of high-dose-rate brachytherapy accidents," *Ann. ICRP*, vol. 35, no. 2, p. 1, 2005.

[2] K. Wallner, J. Blasko, and M. Dattoli, *Prostate Brachytherapy Made Complicated*. Canaan, NY, USA: SmartMedicine Press, 2001.

[3] S. Kang, R. Chou, R. Dodge, R. Clough, H. Kang, M. Bowen, B. Steffey, S. Das, S. Zhou, and A. Whitehurst *et al.*, "Acute urinary toxicity following transperineal prostate brachytherapy using a modified quimby loading method," *Int. J. Radiation Oncology* Biology* Physics*, vol. 50, no. 4, pp. 937–945, 2001.

[4] L. Eapen, C. Kayser, Y. Deshaies, G. Perry, C. Morash, J. Cygler, D. Wilkins, and S. Dahrouge *et al.*, "Correlating the degree of needle trauma during prostate brachytherapy and the development of acute urinary toxicity," *Int. J. Radiation Oncology* Biology* Physics*, vol. 59, no. 5, pp. 1392–1394, 2004.

[5] C. Vargas, M. Ghilezan, M. Hollander, G. Gustafson, H. Korman, J. Gonzalez, and A. Martinez, "A new model using number of needles and androgen deprivation to predict chronic urinary toxicity for high or low dose rate prostate brachytherapy," *J.Urology*, vol. 174, no. 3, pp. 882–887, 2005.

[6] R. Munarriz, Q. Yan, A. Nehra, D. Udelson, and I. Goldstein, "Blunt trauma: The pathophysiology of hemodynamic injury leading to erectile dysfunction," *J. Urology*, vol. 153, no. 6, pp. 1831–1840, 1995.

[7] B. Fisch, B. Pickett, V. Weinberg, and M. Roach, "Dose of radiation received by the bulb of the penis correlates with risk of impotence after three-dimensional conformal radiotherapy for prostate cancer," *Urology*, vol. 57, no. 5, pp. 955–959, 2001.

[8] G. Merrick, K. Wallner, W. Butler, R. Galbreath, J. Lief, and M. Benson, "A comparison of radiation dose to the bulb of the penis in men with and without prostate brachytherapy-induced erectile dysfunction," *Int. J. Radiation Oncology* Biology* Physics*, vol. 50, no. 3, pp. 597–604, 2001.

[9] J. Cunha, I. Hsu, and J. Pouliot, "Dosimetric equivalence of nonstandard HDR brachytherapy catheter patterns," *Med. Phys.*, vol. 36, p. 233, 2009.

[10] Y. Kim, I. Hsu, and J. Pouliot, "Measurement of craniocaudal catheter displacement between fractions in computed tomography-based high dose rate brachytherapy of prostate cancer," *J. Appl. Clin. Med. Phys.*, vol. 8, no. 4, pp. 2415–2415, 2007.

[11] T. Siauw, A. Cunha, A. Atamturk, I.-C. Hsu, J. Pouliot, and K. Goldberg, "IPIP: A new approach to inverse planning for HDR brachytherapy by directly optimizing dosimetric indices," *Med. Phys.*, vol. 38, no. 7, pp. 4045–4051, 2011.

[12] T. Siauw, A. Cunha, D. Berenson, A. Atamtürk, I. Hsu, K. Goldberg, and J. Pouliot, "NPIP: A skew line needle configuration optimization system for HDR brachytherapy," *Med. Phys.*, vol. 39, no. 7, p. 4339, 2012.

[13] D. Stoianovici, K. Cleary, A. Patriciu, D. Mazilu, A. Stanimir, N. Craciunoiu, V. Watson, and L. Kavoussi, "AcuBot: A robot for radiological interventions," *IEEE Trans. Robot. Autom.*, vol. 19, no. 5, pp. 927–930, Oct. 2003.

[14] R. H. Taylor and D. Stoianovici, "Medical robotics in computer-integrated surgery," *IEEE Trans. Robot. Autom.*, vol. 19, no. 5, pp. 765–781, 2003.

[15] A. Vilchis, J. Troccaz, P. Cinquin, K. Masuda, and F. Pellissier, "A new robot architecture for tele-echography," *IEEE Trans. Robot. Autom.*, vol. 19, no. 5, pp. 922–926, Oct. 2003.

[16] A. Salerno, J. Zhang, A. Bhatla, O. V. Lyulko, A. Dutta, G. Garty, N. Simaan, G. Pehrson, Y. L. Yao, D. Brenner, and J. Nie, "Design considerations for a minimally invasive high-throughput automation system for radiation biodosimetry," in *Proc. IEEE Int. Conf. Autom. Sci. Eng., CASE'07*, 2007, pp. 846–852.

[17] K. Liu, N. Gebraeel, and J. Shi, "A data-level fusion model for developing composite health indices for degradation modeling and prognostic analysis," *IEEE Trans. Autom. Sci. Eng.*, vol. 10, no. 3, pp. 652–664, Jul. 2013.

[18] A. Caruso, T. Bouillon, P. Schumacher, E. Zanderigo, and M. Morari, "Control of drug administration during monitored anesthesia care," *IEEE Trans. Autom. Sci. Eng.*, vol. 6, no. 2, pp. 256–264, Apr. 2009.

[19] A. M. Okamura, M. J. Mataric, and H. I. Christensen, "Medical and health-care robotics," *IEEE Robot. Autom. Mag.*, vol. 17, no. 3, pp. 26–37, Sep. 2010.

[20] Y. Yu, J. Zhang, R. Brasacchio, P. Okunieff, D. Rubens, J. Strang, A. Soni, and E. Messing, "Automated treatment planning engine for prostate seed implant brachytherapy," *Int. J. Radiation Oncology* Biology* Physics*, vol. 43, no. 3, pp. 647–652, 1999.

[21] M. Lahanas, D. Baltas, and N. Zamboglou, "Anatomy-based three-dimensional dose optimization in brachytherapy using multiobjective genetic algorithms," *Med. Phys.*, vol. 26, p. 1904, 1999.

[22] E. Lessard and J. Pouliot, "Inverse planning anatomy-based dose optimization for HDR-brachytherapy of the prostate using fast simulated annealing algorithm and dedicated objective function," *Med. Phys.*, vol. 28, p. 773, 2001.

[23] R. Alterovitz, E. Lessard, J. Pouliot, I. Hsu, J. OBrien, and K. Goldberg, "Optimization of HDR brachytherapy dose distributions using linear programming with penalty costs," *Med. Phys.*, vol. 33, p. 4012, 2006.

[24] A. Karabis, P. Belotti, and D. Baltas, "Optimization of catheter position and dwell time in prostate HDR brachytherapy using hipo and linear programming," in *Proc. World Congr. Med. Phys. Biomed. Eng.*. Munich, Germany: Springer, Sep. 7–12, 2009, pp. 612–615.

[25] A. Majewicz, S. Marra, M. van Vledder, M. Lin, M. Choti, D. Song, and A. Okamura, "Behavior of tip-steerable needles in ex vivo and in vivo tissue.," *IEEE Trans. Bio-Med. Eng.*, Oct. 2012.

[26] R. Alterovitz, A. Lim, K. Goldberg, G. S. Chirikjian, and A. M. Okamura, IEEE, "Steering flexible needles under Markov motion uncertainty," in *Proc. IEEE/RSJ Int. Conf. Intell. Robot. Syst. (IROS'05)*, 2005, pp. 1570–1575.

[27] V. Duindam, J. Xu, R. Alterovitz, S. Sastry, and K. Goldberg, "Three-dimensional motion planning algorithms for steerable needles using inverse kinematics," *Int. J. Robot. Res.*, vol. 29, no. 7, pp. 789–800, 2010.

[28] J. Van Den Berg, S. Patil, R. Alterovitz, P. Abbeel, and K. Goldberg, "LQG-based planning, sensing, control of steerable needles," in *Algorithmic Foundations of Robotics IX.*. New York, NY, USA: Springer, 2011, pp. 373–389.

[29] J. Xu, V. Duindam, R. Alterovitz, J. Pouliot, J. Cunha, I.-C. Hsu, and K. Goldberg, "Planning fireworks trajectories for steerable medical needles to reduce patient trauma," in *IEEE/RSJ Inte. Conf. Intell. Robot. Syst., IROS'09*, 2009, pp. 4517–4522.

[30] R. Alterovitz and K. Goldberg, "Motion planning in medicine: Optimization and simulation algorithms for image-guided procedures," *Springer Tracts in Advanced Robotics*, vol. 50, 2008.

[31] K. Reed, A. Majewicz, V. Kallem, R. Alterovitz, K. Goldberg, N. Cowan, and A. Okamura, "Robot-assisted needle steering," *IEEE Robot. Autom. Mag.*, vol. 18, no. 4, pp. 35–46, 2011.

[32] C. Schneider, A. Okamura, and G. Fichtinger, IEEE, "A robotic system for transrectal needle insertion into the prostate with integrated ultrasound," in *Proc. IEEE Int. Conf. Robot. Autom.*, 2004, vol. 1, pp. 365–370.

[33] L. Phee, D. Xiao, J. Yuen, C. Chan, H. Ho, C. Thng, C. Cheng, and W. Ng, IEEE, "Ultrasound guided robotic system for transperineal biopsy of the prostate," in *Proc. IEEE Int. Conf. Robot. Autom.*, 2005, pp. 1315–1320.

[34] G. Fichtinger, E. Burdette, A. Tanacs, A. Patriciu, D. Mazilu, L. Whitcomb, and D. Stoianovici, "Robotically assisted prostate brachytherapy with transrectal ultrasound guidance-phantom experiments," *Brachytherapy*, vol. 5, no. 1, pp. 14–26, 2006.

[35] N. Hungr, J. Troccaz, N. Zemiti, and N. Tripodi, IEEE, "Design of an ultrasound-guided robotic brachytherapy needle-insertion system," in *Proc. IEEE Int. Conf. Eng. Med. Bio. Soc.*, 2009, pp. 250–253.

[36] Y. Yu, T. Podder, Y. Zhang, W. Ng, V. Misic, J. Sherman, D. Fuller, D. Rubens, J. Strang, and R. Brasacchio *et al.*, "Robotic system for prostate brachytherapy," *Comput. Aided Surgery*, vol. 12, no. 6, pp. 366–370, 2007.

[37] A. Patriciu, D. Petrisor, M. Muntener, D. Mazilu, M. Schär, and D. Stoianovici, "Automatic brachytherapy seed placement under MRI guidance," *IEEE Trans. Bio-Med. Eng.*, vol. 54, no. 8, p. 1499, Aug. 2007.

[38] A. Trejos, R. Patel, and R. Malthaner, IEEE, "A device for robot-assisted minimally-invasive lung brachytherapy," in *Proc. IEEE Int. Conf. Robot. Autom.*, 2006, pp. 4187–4192.

[39] S. Salcudean, T. Prananta, W. Morris, and I. Spadinger, IEEE, "A robotic needle guide for prostate brachytherapy," in *Proc. IEEE Int. Conf. Robot. Autom.*, 2008, pp. 2975–2981.

[40] G. Fichtinger, J. Fiene, C. Kennedy, G. Kronreif, I. Iordachita, D. Song, E. Burdette, and P. Kazanzides, "Robotic assistance for ultrasound-guided prostate brachytherapy," *Med. Image Anal.*, vol. 12, no. 5, pp. 535–545, 2008.

[41] R. Pollock, P. Mozer, T. Guzzo, J. Marx, B. Matlaga, D. Petrisor, B. Vigaru, S. Badaan, D. Stoianovici, and M. Allaf, "Prospects in percutaneous ablative targeting: Comparison of a computer-assisted navigation system and the acubot robotic system," *J. Endourology*, vol. 24, no. 8, pp. 1269–1272, 2010.

[42] S. Badaan, D. Petrisor, C. Kim, P. Mozer, D. Mazilu, L. Gruionu, A. Patriciu, K. Cleary, and D. Stoianovici, "Does needle rotation improve lesion targeting?," *Int. J. Med. Robot. Comput. Assisted Surgery*, vol. 7, no. 2, pp. 138–147, 2011.

[43] J. Long, N. Hungr, M. Baumann, J. Descotes, M. Bolla, J. Giraud, J. Rambeaud, and J. Troccaz, "Development of a novel robot for transperineal needle based interventions: Focal therapy, brachytherapy and prostate biopsies," *J. Urology*, 2012.

[44] A. Garg, T. Siauw, D. Berenson, A. Cunha, I.-C. Hsu, J. Pouliot, D. Stoianovici, and K. Goldberg, "Initial experiments toward automated robotic implantation of skew-line needle arrangements for HDR brachytherapy," in *Proc. IEEE Conf. Autom. Sci. Eng.*, Aug. 2012, pp. 26–33.

[45] I. Hsu, K. Bae, K. Shinohara, J. Pouliot, J. Purdy, G. Ibbott, J. Speight, E. Vigneault, R. Ivker, and H. Sandler *et al.*, "Phase II trial of combined high-dose-rate brachytherapy and external beam radiotherapy for adenocarcinoma of the prostate: Preliminary results of RTOG 0321," *Int. J. Radiation Oncology* Biology* Physics*, vol. 78, no. 3, pp. 751–758, 2010.

[46] K. Arun, T. Huang, and S. Blostein, "Least-squares fitting of two 3-D point sets," *IEEE Trans. Pattern Anal. Mach. Intell.*, no. 5, pp. 698–700, Sep. 1987.

[47] M. Uecker, S. Zhang, D. Voit, A. Karaus, K.-D. Merboldt, and J. Frahm, "Real-time MRI at a resolution of 20 ms," *NMR Biomed.*, vol. 23, no. 8, pp. 986–994, 2010.

[48] S. Zhang, K. T. Block, and J. Frahm, "Magnetic resonance imaging in real time: Advances using radial flash," *J. Magn. Resonance Imaging*, vol. 31, no. 1, pp. 101–109, 2010.

[49] S. Tovar-Arriaga, R. Tita, J. C. Pedraza-Ortega, E. Gorrostieta, and W. A. Kalender, "Development of a robotic FD-CT-guided navigation system for needle placement—Preliminary accuracy tests," *Int. J. Med. Robot. Comput. Assisted Surgery*, vol. 7, no. 2, pp. 225–236, 2011.

[50] W. Ji, "Reconfigurable fiducial-integrated modular needle driver for MRI-guided percutaneous interventions," M.S. thesis, Worcester Polytechnic Institute, Worcester, MA, USA, 2013.

[51] Y.-L. Park, S. Elayaperumal, B. Daniel, S. C. Ryu, M. Shin, J. Savall, R. Black, B. Moslehi, and M. Cutkosky, "Real-time estimation of 3-d needle shape and deflection for MRI-guided interventions," *IEEE/ASME Trans. Mechatronics*, vol. 15, no. 6, pp. 906–915, Dec. 2010.

[52] R. Seifabadi, N. B. J. Cho, S.-E. Song, J. Tokuda, N. Hata, C. M. Tempany, G. Fichtinger, and I. Iordachita, "Accuracy study of a robotic system for MRI-guided prostate needle placement," *Int. J. Med. Robot. Comput. Assisted Surgery*, 2012.

Animesh Garg (S'13) received the BSc.(Eng.) degree in manufacturing processes and automation from the University of Delhi, Delhi, India, in 2010, and the M.S. degree in industrial engineering from the Georgia Institute of Technology, Atlanta, GA, USA, in 2011. He is currently working towards the Ph.D. degree at the Department of Industrial Engineering and Operations Research, University of California (UC Berkeley), Berkeley, CA, USA.

He currently works in the area of optimization and machine learning with applications in radiotherapy, robotics and computer assisted surgery.

Timmy Siauw received the B.S., M.S., and the Ph.D. degree in civil systems and environmental engineering from the University of California (UC Berkeley), Berkeley, CA, USA in 2006, 2008, and 2012, respectively.

He is a Postdoctoral Scholar with the Physics Division of the University of California, San Francisco, CA, USA. His concentration is applications of mathematical programming to radiotherapy planning.

Dmitry Berenson (M'12) received the Ph.D. degree at the Robotics Institute, Carnegie Mellon University (CMU), Pittsburgh, PA, USA, in 2011, where his advisors were S. Srinivasa and J. Kuffner.

He worked in the Personal Robotics Lab and completed interships at the Digital Human Research Center, Japan, Intel Labs, Pittsburgh, and LAAS-CNRS, France. In 2012, he completed a Postdoctoral at UC Berkeley working with K. Goldberg and P. Abbeel. He is now an Assistant Professor at Worcester Polytechnic Institute (WPI) in the Robotics Engineering Program and Computer Science Department, where he founded the Autonomous Robotic Collaboration (ARC) Lab at WPI, which focuses on motion planning, manipulation, and human-robot collaboration.

J. Adam M. Cunha received the Ph.D. degree from the University of California, Santa Barbara, CA, USA, in 2006.

He is an Assistant Professor of Medical Physics with the Department of Radiation Oncology, University of California, San Francisco, CA, USA. Since 2009, he has been on the Executive Board of the Bay Area Chapter of the American Association of Physicists in Medicine (AAPM) in the capacity of President and President Emeritus. He is currently a member of the AAPM Task Group No. 192, Guidelines for Image-Guided Robotic Brachytherapy.

I-Chow (Joe) Hsu received the M.D. degree from Johns Hopkins School of Medicine, Baltimore, MD, USA, and completed a residency in radiation oncology at Columbia-Presbyterian Medical Center, New York, NY, USA.

He is an expert in brachytherapy. He specializes in the treatment of genitourinary, gynecological, head and neck and soft tissue tumors. He is interested in the development of minimally invasive implant procedures and precision delivery of conformal high dose rate brachytherapy and hyperthermia.

Jean Pouliot is Director of the Physics Division, Vice Chair and Professor of Radiation Oncology at the University of California, San Francisco, CA, USA, with a joint appointment with the Graduate Bioengineering UC Berkeley—UCSF program. He is author and coauthor of more than 160 peer-reviewed publications.

Prof. Pouliot was voted among the Top 25 Innovators in the U.S., Health Imaging and IT, in June 2006 for his pioneering research on MegaVoltage Cone Beam CT imaging.

Dan Stoianovici (M'XX) is a Professor of Urology, Mechanical Engineering, and Neurosurgery at the Johns Hopkins University, Baltimore, MD, USA. He is the Director of the Urology Robotics Program and teaches computer-aided design.

Dr. Stoianovici is the Executive Director of the Engineering and Urology Society, serves on the editorial boards of the *Journal of Endourology*, the IEEE/ASME TRANSACTIONS ON MECHATRONICS, the *International Journal of Medical Robotics and Computer Aided Surgery*, and serves on the National Institute of Health study sections.

Ken Goldberg (F'05) received the Ph.D. degree in computer science from Carnegie Mellon University (CMU), Pittsburgh, PA, USA, 1990.

He is a Professor of Industrial Engineering and Operations Research at the University of California (UC Berkeley), Berkeley, CA, USA, with appointments in Electrical Engineering and Computer Science, School of Information, and Art Practice at UC Berkeley and Radiation Oncology at University of California (UC San Franciso), San Francisco, CA, USA. He has published over 170 refereed papers and awarded eight U.S. patents.

Prof. Goldberg was awarded the NSF Presidential Faculty Fellowship in 1995, the Joseph Engelberger Award for Robotics Education in 2000, and the IEEE Major Educational Innovation Award in 2001. He is Founding Co-Chair of the IEEE Technical Committee on Networked Robots and Co-Founder of T-ASE. He served as Vice-President of Technical Activities for the IEEE Robotics and Automation Society (2006–2009) and is Editor-in-Chief of the IEEE TRANSACTIONS ON AUTOMATION SCIENCE AND ENGINEERING (T-ASE).